Accepted Manuscript
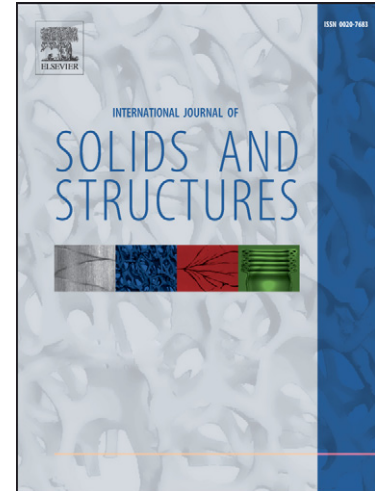
Interaction of Highly Nonlinear Solitary Waves with Thin Plates

Jinkyu Yang, Devvrath Khatri, Paul Anzel, Chiara Daraio

Please cite this article as: Yang, J., Khatri, D., Anzel, P., Daraio, C., Interaction of Highly Nonlinear Solitary Waves with Thin Plates, *International Journal of Solids and Structures* (2012), doi: 10.1016/j.ijsolstr.2012.02.013

Interaction of Highly Nonlinear Solitary Waves with Thin Plates

Jinkyu Yang[1,2], Devvrath Khatri[1], Paul Anzel[1], and Chiara Daraio[1*]

Engineering and Applied Science, California Institute of Technology
1200 E. California Blvd., MC 105-50, Pasadena, California 91125, USA

Mechanical Engineering Department, University of South Carolina
300 Main Street, A224, Columbia, South Carolina 29208, USA

ABSTRACT

We investigate the reflection of highly nonlinear solitary waves in one-dimensional granular crystals interacting with large plates. We observe significant changes in the reflected waves' properties in terms of wave amplitude and time of flight in association with the intrinsic inelasticity of large plates, which are governed by the plate thickness and the size of the granular constituents. We also study the effects of fixed plate boundaries in the formation of reflected waves, and find the existence of a critical distance, within which the interaction between the granular chain and plate is strongly modified. We explain the effects of intrinsic inelasticity and of boundaries in the large plates by using plate theory and the contact mechanics between a plate and a spherical striker. We find that experimental results are in excellent agreement with the analytical predictions and numerical simulations based on the combined discrete element and spectral element models. The findings in this study can be useful for the nondestructive evaluation of plate structures using granular crystals, which can improve the resolution of *in-situ*, portable measurement instruments leveraging high acoustic energy and sensitivity of solitary waves.

* Corresponding author: daraio@caltech.edu, Tel.: +1 626-395-4479, Fax: +1 626-449-6359

1. Introduction

Granular crystals are aggregates of tightly packed elements whose macroscopic properties are strongly determined by their underlying architecture. For example, ordered arrays of discrete, elastic particles can exhibit remarkable versatility in their wave dynamics depending on their materials, geometry, and boundary conditions (Nesterenko, 1983; Sinkovits and Sen, 1995; Hladky-Hennion and de Billy, 2007; Tournat and Gusev, 2010). One-dimensional (1D) granular crystals composed of spherical particles under zero or weak static compression have been shown to support the generation and propagation of compactly-supported nonlinear waves, called solitary waves (Nesterenko, 1983, 2001). Compared to linear elastic waves in continuous media, these nonlinear waves present unique physical properties: They can support high acoustic energy at a constant spatial wavelength, and their speed can be tuned by varying the system's parameters (static precompression, materials properties, and geometry) (Coste et al., 1997; Nesterenko, 2001; Daraio et al., 2006b). The propagation speed of solitary waves is an order-of-magnitude slower than the dilational waves within the spheres that compose the granular crystals and shows a strong dependence on their amplitudes (Nesterenko, 2001; Daraio et al., 2006b). By exploiting these characteristics, previous studies have reported potential applications of granular crystals in shock mitigation (Sen et al., 2001; Hong, 2005; Daraio et al., 2006; Melo et al., 2006), acoustic imaging (Sen et al., 1998, 2005; Spadoni and Daraio, 2010), and nondestructive evaluation devices (Khatri et al., 2008; Ni et al., 2011; Yang et al., 2012).

To design engineering tools based upon the distinctive wave dynamics in granular crystals, we need to have an understanding of the interaction of granular crystals with neighboring structures. This is particularly crucial for developing granular crystal-based sensor devices which employ solitary waves to inspect structural systems nondestructively. Previous work has been limited to one-dimensional studies, exploring the interaction of the solitary waves in granular crystals with an adjacent simple, linear elastic medium (Job et al., 2005; Yang et al., 2011). Based on discrete particle dynamics and elastic contact theory, these works have successfully validated the coupling mechanism between nonlinear granular crystals and the linear media. In particular, they have reported that the reflected solitary waves can be disintegrated into a chain of secondary solitary waves whose propagation speed and attenuation are significantly affected by the bounding medium's mechanical properties. To the authors' knowledge, however, no rigorous work has been done on the interaction of 1D granular crystals with plate structures. This three-dimensional interaction exhibits more complex coupling behavior between nonlinear granular systems and linear elastic plate structures stemming from the dispersive wave dynamics and a strong dependence upon boundary effects in plates.

The purpose of the present study is to provide experimental, numerical, and analytical groundwork on the interaction of nonlinear granular crystals with large plates. We perform an

2

experimental parametric study, varying the size of granular crystals and the thickness of large plates to investigate how incident solitary waves in granular crystals are reflected at the plate interface in association with their geometric configurations. To verify the experimental results, we numerically simulate the wave dynamics between the nonlinear granular crystals and the linear elastic plates by means of a combined discrete element model (DEM) and spectral element model (SEM). We report that the response of solitary waves is highly sensitive to the thickness of the plate relative to the sphere size of granular crystals. In particular, we numerically verify that the reflected solitary waves can exhibit a significant amount of wave attenuation and time delay without the inclusion of plasticity and viscoelastic effect. To analytically explain this intrinsic inelasticity in the combined granular and plate system, we use the classical theory of contact mechanics upon solid sphere impact and the subsequent wave dynamics in plates (Zener, 1941; Sondergaard et al., 1990). We also report that the reflected solitary waves in granular chains are significantly affected by the proximity to the plate's fixed support within some critical distance. By calculating the travelling distance of the generated waves in the plate during the estimated interaction time between the granular chain and the plate, we derive the critical distance in association with the granular crystal and plate geometry.

The sensitive response of the solitary waves to the geometrical configurations and boundary conditions of the plates implies that 1D granular crystals can be employed in inspecting structural systems in a fast and nondestructive manner. The sensing scheme based on solitary waves can provide unique advantages over conventional nondestructive evaluation techniques that use ultrasounds. For example, solitary waves formed in granular crystals can easily achieve higher intensity of stress waves than ultrasonic waves excited by conventional piezoelectric actuators, because they rely on mechanical impacts for excitation rather than piezoelectric conversion efficiencies (Spadoni and Daraio, 2010). This may lead to improved signal-to-noise ratios and reliability of granular crystal-based sensors. In addition, the 1D granular crystals are compact and do not rely on external power amplifiers for generating excitation waves. Thus, it is possible to enhance the portability and accessibility of a sensing instrument using granular crystals.

This paper is organized as follows: First, we describe the experimental setup of the combined granular chain and large plate in Sec. 2. We then introduce a numerical model that simulates the interaction of the solitary waves in granular chains with the large plate in Sec. 3. In Sec. 4, we explain the coupling mechanism using an analytical approach based on classical contact mechanics and wave dynamics in plates, and we compare the analytical results with the numerical and experimental results. Lastly, in Sec. 5, we conclude the manuscript with a summary and the implications of our work.

2. Experimental setup

3

The overall configuration of the experimental setup is shown in Fig. 1. The test setup consists of a horizontal thin plate rigidly clamped at two opposing edges and a 1D vertical granular chain positioned on the top of the plate. The last particle of the granular chain rests on the plate. In this study, we assemble three different chains with spheres of diameter $D = [4.76, 9.53, 19.1]$ mm. Each granular chain is composed of 20 stainless steel particles (type-440C, elastic modulus $E_s = 200$ GPa, Poisson's ratio $v_s = 0.28$, and density $\rho_s = 7,800$ kg/m³) guided by four steel rods. We generate a single solitary wave in the granular chain by the impact of a spherical striker identical to the particles composing the granular chain (Nesterenko, 2001). For repeatability of the impact, the striker is released from a drop height of 5 mm using a solenoid (Yang et al., 2011). We assume negligible effect of air drag on the striker during the drop, obtaining an impact speed of $\upsilon_{imp} = 0.31$ m/s with only a 0.45% standard deviation in the velocity distribution. The propagation of solitary waves is measured by a sensor particle positioned on the 7th particle location from the top of the granular crystal, which has an embedded calibrated piezoelectric transducer [inset of Fig. 1]. A detailed procedure for the assembly and calibration of this sensor particle can be found in (Daraio et al., 2005). The sensor particle's total mass is approximately equal to that of the other beads in the chain and does not affect the propagation of the solitary waves (Nesterenko, 2001; Job et al., 2007; Sokolow et al., 2007).

We use three aluminum plates (Alloy 6061, 914 × 914 mm) with thicknesses $t = [2.29, 3.18, 4.83]$ mm. The elastic modulus, Poisson's ratio, and density of the aluminum plates are $E_p = 68.9$ GPa, $v_p = 0.33$, and $\rho_p = 2,360$ kg/m³ respectively. To investigate the coupling behavior between the granular chain and the plate, we vary the position of the granular chain along the centerline of the plate in the direction of the fixed support [Fig. 1]. The distance between the granular chain and the support is incremented 10 mm up to 200 mm distance from the support and 20 mm afterwards up to the center of the panel. Measured signals of incident and reflected solitary waves are digitized and transferred to a computer using a data acquisition device. Testing is repeated five times at every location to obtain a statistical distribution of measurement results.

3. Numerical approach

In this study, we employ a discrete element model (DEM) for describing the nonlinear wave dynamics in the granular crystal, and a spectral element model (SEM) for simulating wave propagation in a thin plate. These two models are integrated together at the contact interface to describe the coupling behavior between the nonlinear granular chain and the linear elastic plate.

3.1. *Discrete element model*

The formation and propagation of solitary waves can be successfully simulated using a DEM that approximates a 1D granular crystal as a chain of point masses connected by nonlinear springs (Nesterenko, 2001). In this model, the interaction between the particles is described by the Hertzian contact law $F \propto \delta^{3/2}$, where F is the compressive force and δ is the displacement approach between particles (Johnson, 1985). The equation of motion for the nth spherical particle can be written as:

$$m\ddot{u}_n = A_n[u_{n-1} - u_n]_+^{3/2} - A_{n+1}[u_n - u_{n+1}]_+^{3/2} + mg, \quad n \in \{1, \ldots, N\},$$

$$A_n \equiv \begin{cases} A\big|_s = \dfrac{E_s\sqrt{D}}{3(1-v_s^2)} & n \in \{1, \ldots, N\} \\[3mm] A\big|_p = \dfrac{2}{3}\sqrt{2D}\left(\dfrac{1-v_s^2}{E_s} + \dfrac{1-v_p^2}{E_p}\right)^{-1} & n = N+1 \end{cases} \tag{1}$$

Here, m is the particle mass, u_n is the displacement of nth particle from its equilibrium position (with no pre-load), and g is the acceleration of gravity applied to the particle. The bracket $[s]_+$ denotes $max(s, 0)$, implying no support of a tensile force between particles. Combined with the nonlinear Hertzian contact force under compression, this zero tensile force constitutes a double nonlinearity in the system (Nesterenko, 2001). The total number of the particles in the granular crystal is $N = 20$ in this study, and the striker is represented by $n = 0$ [Fig. 2(a)]. The coefficients $A\big|_s$ and $A\big|_p$ are stiffness values in the chain (i.e., between spheres) and at the interface (i.e., between the last sphere and the plate) respectively. According to Eq. (1), the dynamics of the last particle in the chain ($n = N$) is affected by the Hertzian contact force exerted by the plate:

$$f^{ext} = A\big|_p[u_N - u_{N+1}]_+^{3/2}, \tag{2}$$

where u_{N+1} denotes the plate's displacement at the contact point [Fig. 2(a)].

3.2. *Spectral element model*

The spectral element model (SEM) is an advanced form of the finite element model (FEM) for minimizing numerical errors and reducing computation time (Patera, 1984). Previous studies have reported a significantly faster convergence of solution using SEM in both spatial and temporal domains compared to the classical FEM (Kim et al., 2008). In particular, the SEM has proven to be highly effective in simulating wave dynamics in thin plate structures, capturing Lamb wave propagation with minimal dispersive error.

The displacement fields in SEM are characterized by higher-order nodal basis functions defined at Gauss-Lobatto-Legendre (GLL) points (Komatitsch et al., 2000). The GLL points are distributed strategically in a local element space [Fig. 2(b)], which is in sharp contrast to the evenly spaced nodes in

FEM. Based on these non-uniformly distributed nodal points, the displacement vector in i-direction (w_i) can be expressed mathematically as:

$$w_i(\xi, \eta, \zeta) = \sum_{p=0}^{N_p} \sum_{q=0}^{N_q} \sum_{r=0}^{N_r} h_p(\xi)\, h_q(\eta)\, h_r(\zeta)\, d_i^{pqr}, \tag{3}$$

where ξ, η, and ζ are local coordinates in spectral elements, and d_i^{pqr} is the displacement at the GLL point with nodal coordinate index (p, q, r). The polynomial $h_p(\xi)$ is an N_pth-order Lagrange interpolation function in the ξ-direction (Patera, 1984; Kim et al., 2008) [Fig. 2(b) shows the 4th-order GLL points in the horizontal direction].

Based on the spectral element method, we use a numerical integration rule called nodal quadrature, where integration points coincide with the nodal (i.e., GLL) points (Ha, 2009). After the nodal quadrature the equation of motion of the plate system can be expressed in the matrix form as:

$$M_{ij}\ddot{d}_j + K_{ij} d_j = F_i^{ext}. \tag{4}$$

The matrices M_{ij} and K_{ij} are the global mass and stiffness matrices and F_i^{ext} is the external force vector. It is notable that in SEM we obtain a diagonal form of mass matrix M_{ij} even without the lumped-mass approximation commonly used in FEM which often harms solution accuracy. This is due to the strategic selection of nodes at GLL points combined with nodal quadrature integration scheme (Patera, 1984; Kim et al., 2008). In addition, the high-order Lagrange polynomials enables us to achieve more accurate shape of element deformation using a reduced number of nodes, compared to evenly spaced nodal points in FEM.

The force vector F_i^{ext} is composed of the force components required to keep the boundary conditions. At the chain-plate contact point, this component corresponds to the compressive force exerted to the plate by the granular chain [f^{ext} in Eq. (2)]. As mentioned in Section 3.1, the Hertzian contact force here is determined by the particle dynamics in the granular chain, and in turn, the reaction of the granular chain is governed by the motion of the plate at the contact point. We numerically solve this coupling mechanism of the granular and elastic system by using a combined scheme of DEM and SEM. We use 256 elements in the plate structure (16×16 in the lateral direction and a single element in the thickness direction). For each element, the order of interpolation function is $N_p = 4$, $N_q = 4$, and $N_r = 2$ (i.e., 5×5×3 nodes per element, 12675 nodes for the whole plate). Note that we use only a single element with the 2nd-order interpolation function in the thickness-direction of the plate. This is based on results that both the first symmetric and asymmetric modes of the Lamb wave propagation in plate structures can be successfully simulated using only 3 nodes in the thickness direction (Ha, 2009). We solve the

6

numerical model of the DEM and SEM by performing the combined Newmark (Zienkiewicz et al., 2005) and Runge-Kutta ('ODE45' function) integration in Matlab®. In this study, we do not take any dissipation effect into account and consequently, assure that the energy initially carried by the striker is conserved throughout the interaction between the granular chain and the plate; we will later show that the attenuation of the reflected solitary waves is primarily attributable to the intrinsic inelasticity of the thin plate rather than any dissipative effects within the granular chain. Figure 2 shows a snapshot of the guided wave propagation in the plate structure under the action of solitary waves from the granular chain.

4. Results and discussion

In this section, we compare the experimental and numerical results with the analytical predictions of solitary wave reflection behavior obtained from the classical plate theory and the contact mechanics. First, we analyze the interaction of granular chains with thin plates in various combinations of sphere size (D) and plate thickness (t). The experiments are conducted with the granular chains positioned at the center of the plate to avoid the effect of the plate boundary conditions. We then move the granular crystals to various points near and away from the fixed plate support to assess the boundary effect.

4.1. Effect of granular crystal and plate geometry

Figure 3 shows the solitary wave profiles measured by the sensor particle for two different plates ($t = 2.29$ and 4.83 mm) using a granular chain with $D = 9.53$ mm. The first impulses around ~0.15 ms represent the incident solitary waves passing by the sensor particle upon the impact of the striker. The subsequent impulses are the reflected waves from the interface, propagating back through the granular chain and arriving at the sensor site. We quantify the time of flight (TOF) of solitary waves by measuring the elapsed time between the incident and reflected waves. The magnitudes of the reflected waves are compared using the amplitude ratios of reflected wave (ARR) to that of the incident solitary wave (F_{ref}/F_{in}).

The reflected solitary waves in this study are formed by the rebounding motion of granules against the plate. Upon the incidence of solitary waves into the interface between the granular chain and the plate, the last particle in the chain collides with the plate and is pushed back towards the rest of the chain by the restitution of the plate. As a result, the thicker plate forms stronger and faster reflected waves, while the thinner plate generates weaker and slower waves, as shown in Fig. 3. The numerical results obtained by the combined DEM and SEM closely resemble the experimental results (compare solid and dotted lines in Fig. 3). Due to the exclusion of dissipative effects within the chain and in the plate in simulation, the magnitudes of simulated solitary waves are larger than those of the experimental

7

signals. However, we find that this does not affect significantly the patterns of wave reflection, particularly in terms of TOF.

The interfacial dynamics between the granular chain and the plate is phenomenologically similar to the classical problem of a single particle impact on a plate. This is due to the discreteness and nonlinearity of granular crystals, in which the propagating energy is concentrated on the particles within the width of compactly-supported solitary waves (approximately five particle diameters for a monodispersed granular chain) (Nesterenko, 2001; Sokolow et al., 2007). In particular, when the solitary wave reaches the interface, the majority of the energy carried by a single pulse of solitary waves is converted to the potential energy between the last particle and the plate. Thus, the interaction between the granular chain and the plate can be approximately modeled as the last particle's impact on the plate in the short duration of contact.

4.1.1. Equation of motion

The normal impact of spheres with flat plates has been analytically studied in the literature (Zener, 1941; Sondergaard et al., 1990). Based on the theory of thin plates under the elastic impact, the dynamic motion of the striker can be described in terms of the dimensionless time (τ) and the dimensionless approach (σ) between the plate and the spherical striker (Zener, 1941):

$$d^2\sigma/d\tau^2 + (1 + \lambda \, d\sigma/d\tau)\sigma^{3/2} = 0 \, ,$$

$$\left. \begin{array}{l} \sigma = 0 \\ d\sigma/d\tau = 1 \end{array} \right\} \quad \text{at} \quad \tau = 0. \tag{5}$$

Zener found that the restitutional motion of the striker depends upon the inelasticity parameter λ, which is determined by the material properties and geometry of both the sphere and the plate:

$$\lambda = \frac{\pi^{3/5}}{4\sqrt{3}} \left(\frac{D}{t}\right)^2 \left(\frac{\rho_s}{\rho_p}\right)^{3/5} \left[\frac{\upsilon_{in}^2 \rho_p (1 - v_p^2)}{E_p}\right]^{1/10} \left[1 + \frac{E_p(1 - v_s^2)}{E_s(1 - v_p^2)}\right]^{-2/5} . \tag{6}$$

Here D and t are the sphere diameter and the plate thickness, and the subscripts s and p denote the properties of spherical striker and the plate respectively. The impact velocity υ_{in} corresponds to the incident speed of the striker at the moment of collision. By solving Eq. (5) given the inelasticity parameter λ, we can analytically calculate the repulsive motion of the striker and as a result, obtain the coefficient of restitution e.

Figure 4(a) shows the calculated restitution coefficient as a function of the inelasticity parameter. If $\lambda \approx 0$ (i.e., $D \ll t$, corresponding to the case that a sphere impacts a half-spaced wall), we obtain perfect rebounding motion of the sphere, leading to $e \approx 1$. If $\lambda \rightarrow \infty$ (i.e., the sphere diameter is much larger than

the plate thickness), the restitution coefficient approaches zero ($e \approx 0$) due to the dominant inertia effect of the striker. Note that the imperfect reflection of the sphere ($e < 1$) is attributed to the energy dispensed to the plate during the impact, not due to any dissipative losses of energy such as plasticity and viscoelasticity. Zener called this the "intrinsic inelasticity" of plates (Zener, 1941).

We also obtain the dimensionless contact time (τ_c) as a function of inelasticity parameter by solving Eq. (5) [Fig. 4(b)]. The dimensionless time shown in Fig. 4(b) can be converted to the contact time T_c between the sphere and the plate by:

$$T_c = m^{2/5} \upsilon_{in}^{-1/5} A\big|_p^{-2/5} \tau_c,$$
(7)

where m is the mass of the sphere and $A\big|_p$ is given in Eq. (1) (Zener, 1941). If the diameter of the sphere is much smaller than the plate thickness ($\lambda \approx 0$), T_c in Eq. (7) approaches the contact time of a sphere against a semi-infinite wall ($\tau_{c,0} \approx 3.22$) (Tillett, 1954; Yang et al., 2011). As the inelasticity parameter increases, the contact time increases due to the weakened restitutional force exerted on the sphere by the plate.

4.1.2. Amplitude ratio of reflected waves (ARR)

Now we investigate the amplitude ratio of reflected solitary waves (ARR) in association with the granular particle size and the plate thickness. One of the unique properties of nonlinear solitary waves is the dependence of their propagating speed on the wave amplitudes, given by $V \propto F^{1/6}$ where V is the solitary wave velocity and F is the maximum force magnitude of the propagating solitary waves. The speed of solitary waves is, in turn, proportional to $\upsilon^{1/5}$ where υ is the maximum particle velocity attained during the propagation of solitary waves (Nesterenko, 2001; Yang et al., 2011). Hence, the amplitude ratio of the reflected solitary waves (ARR) can be expressed as:

$$ARR \equiv \frac{F_{ref}}{F_{in}} = \left(\frac{V_{ref}}{V_{in}}\right)^6 = \left(\frac{\upsilon_{ref}}{\upsilon_{in}}\right)^{6/5},$$
(8)

where subscript '*in*' and '*ref*' represent the incident and reflected solitary waves. If we assume negligible energy dissipation along the chain, the maximum particle velocities is preserved along the chain during the propagation of solitary waves. Thus, the particle velocity ratio can be replaced by the restitution coefficient of the last particle:

$$ARR \approx e^{6/5}.$$
(9)

9

The restitution coefficient e is governed by the inelasticity coefficient λ [see Fig. 4(a)], which is a function of the ratios between the granular crystal diameter (D) and the plate thickness (t) according to Eq. (6). Thus, the ARR values can be plotted as a function of D/t [solid black line in Fig. 5]. We find that the smaller D/t (i.e., a thicker plate or a smaller striker) results in the higher ARR values. As D/t increases, we observe reduced ARR values due to the increase of the inelastic effect. Above $D/t \approx 5$ the ARR values approach zero, producing negligible magnitude of reflected solitary waves. This corresponds to the case that a large-mass sphere impacts a relatively thin plate, and as a result, we observe no significant restitution of the sphere against the plate because of the dominance of sphere's inertial effect. The simulation results are plotted in solid grey marks in Fig. 5, under various combinations of plates ($t =$ [2.29, 3.18, 4.83] mm) and granular crystals ($D =$ [4.76, 9.53, 19.05] mm). We observe that the numerical results corroborate the analytic predictions. The experimental results are also depicted in Fig. 5 (hollow marks), in which the error bars denote the standard deviations from five measurements per test. We observe that the experimental data qualitatively confirm the analytical and numerical results. The discrepancy between the measured ARR values and the analytical/numerical results is attributed to the presence of dissipative effect in experiments, which is ignored in the analytical and numerical approaches in this study.

4.1.3. Time of flight (TOF)

We evaluate the time of flight (TOF) of reflected solitary waves under various geometrical configurations of the granular chains and the bounding plates. The TOF in this study consists of the solitary wave travelling time in the chain (T_t) and the delay time of wave reflection at the interface between the granular chain and the plate (T_c):

$$TOF \equiv T_t + T_c. \tag{10}$$

The delay time T_c can be approximated to the contact time between the last particle and the plate, derived in Eq. (7). On the other hand, the travelling time T_t can be calculated by summing the wave transit time of incident ($T_{t,in}$) and reflected ($T_{t,ref}$) solitary waves, given a distance between the instrumented sensor and the plate. For a 1D chain, this distance is $N \times D$, where N is the number of particles between the sensor and the plate and D is the particle diameter ($N = 14$ in this study). Consequently, the travelling time can be expressed as:

$$T_t = T_{t,in} + T_{t,ref} = \frac{ND}{V_{in}} + \frac{ND}{V_{ref}}. \tag{11}$$

Using Nesterenko's long-wave approximation, the solitary wave speed in an uncompressed 1D monodispersed chain can be analytically expressed as (Nesterenko, 2001; Yang et al., 2011):

$$V_{in} = (16/25)^{1/5} D (\upsilon_{in} A\big|_s^2 / m^2)^{1/5}. \tag{12}$$

According to Chatterjee's numerical investigations, the maximum particle velocity under solitary wave propagation in a monoatomic chain can be expressed as $\upsilon_{in} \approx 0.682 \upsilon_{imp}$ where υ_{imp} is the velocity of the striker identical to the particles in the chain (Chatterjee, 1999). Thus, the travelling time of the incident solitary wave becomes:

$$T_{t,in} \approx 1.180 N \ m^{2/5} \upsilon_{imp}^{-1/5} A\big|_s^{-2/5}. \tag{13}$$

From Eq. (11) and using $V_{in}/V_{ref} = (\upsilon_{in}/\upsilon_{ref})^{1/5} = e^{-1/5}$ [Eq. (8)], the total travelling time of solitary waves is:

$$T_t = \frac{ND}{V_{in}} + \frac{ND}{V_{ref}} = T_{t,in}\left(1 + \frac{V_{in}}{V_{ref}}\right)$$
$$\approx 1.180\left(1 + e^{-1/5}\right) N \ m^{2/5} \upsilon_{imp}^{-1/5} A\big|_s^{-2/5} \tag{14}$$

Plugging Eqs. (7) and (14) into Eq. (10), the total time of flight becomes:

$$TOF = [1.180(1 + e^{-1/5}) N A\big|_s^{-2/5} + 1.080 \, \tau_c A\big|_p^{-2/5}] \, m^{2/5} \upsilon_{imp}^{-1/5}. \tag{15}$$

The analytical results of TOF based on Eq. (15) are shown in Fig. 6(a) for three different plate thicknesses. Unlike the ARR curve in Fig. 5, the TOF results are not solely a function of D/t but exhibit distinctive values for different plate thicknesses. This means that we obtain further delay of solitary wave reflection if the size of the granular crystal increases (large D) or the thickness of the plate decreases (small t). The reduction of the plate thickness contributes to the elongation of the contact time (T_c) due to the inelasticity effect from the plate. On the contrary, a larger particle size results in the increase of both the wave travelling time (T_t) by lengthening the wave travel distance and the contact time (T_c) by enhancing the inertia effect. This becomes more evident if we normalize TOF with respect to the sphere diameter D:

$$TOF/D = \left[1.414(1 + e^{-1/5}) N \left(\frac{1-v_s^2}{E_s}\right)^{2/5} + 0.853 \tau_c \left(\frac{1-v_s^2}{E_s} + \frac{1-v_p^2}{E_p}\right)^{2/5}\right] \rho_s^{2/5} \upsilon_{imp}^{-1/5}. \tag{16}$$

We find that the normalized TOF become a sole function of D/t because both e and τ_c in Eq. (16) are governed by λ, which is in turn a function of D/t.

The normalized TOF is plotted in Fig. 6(b) (solid black line). We find that the three separate curves in Fig. 6(a) are now collapsed seamlessly into a single curve and both numerical (filled marks) and experimental (hollow marks) results are in excellent agreement with the analytical results. The deviation of the rightmost point, which corresponds to the heaviest sphere impact on a thinnest plate, is possibly

11

due to the effect of guided waves in plate reflected from the fixed support during the relatively long contact time between the large granular particles and the thin plate. This boundary effect is discussed in the next Section.

4.2. Effect of plate boundary

4.2.1. Amplitude ratio of wave reflection (ARR) and time of flight (TOF)

To evaluate the boundary effect, we position granular chains at various distances L from the support [see Fig.1]. Similar to the previous section, we transmit a single solitary wave and measure the magnitudes and delay time of reflected waves in terms of ARR and TOF in each experiment. The experimental and numerical values of the ARR are reported in Figs. 7(a) and (b) for $D = 9.53$ and 19.05 mm respectively as a function of a distance from the support. We observe that the reflected waves exhibit high ARR values (strong reflection) if the granular crystal is positioned close to the support. Particularly, in numerical simulations under no dissipation, the ARR values approach one meaning a highly elastic interaction between the granular crystal and the plate near the support. As the distance from the support increases the ARR values decrease and, after a critical distance, the ARR values become approximately constant. Note that the distinction between three curves corresponding to different plate thicknesses is not clear in Fig. 7(b) [$D = 19.1$ mm] compared to Fig. 7(a) [$D = 9.53$ mm]. This is due to the dominant effect of granular particles' inertia, as confirmed by the low ARR values measured after the critical distances from the boundaries. The experimentally measured ARR values are smaller than the ones obtained from the numerical simulations [compare the filled and hollow marks in Figs. 7(a) and (b)]. This is again attributed to the existence of dissipative effects in experiments such as friction, viscoelasticity, and plasticity.

We can similarly plot the variation of TOF values as a function of the distance from the support [Fig. 8]. Again, we observe a clear effect of boundaries: Within the critical distance, we observe that the TOF values respond sensitively to the distance from the support. For the chain positioned near the support ($L \approx 0$), the measured TOF values are around ~0.5 ms in Fig. 8(a) and ~1 ms in Fig. 8(b), regardless of the plate thickness. This is due to the reinforced plate stiffness near the fixed support. As the distance increases the plate behaves more inelastically, leading to the increase in the TOF values. This boundary effect becomes more evident for the interaction with a larger granular chain ($D = 19.05$ mm) [compare the y-axis scales of Figs. 8(a) and (b)]. We also observe that the critical distance is strongly influenced by the plate thickness; the TOF values are stabilized around 0.05 m for the thickest plate ($t = 4.83$ mm), while the thinnest plate ($t = 2.29$ mm) shows a much longer range of boundary effect with the critical distance at ~0.15 m.

4.2.2. Critical distance

The existence of critical distance can be explained by the propagation and reflection of the guided waves in the plate. If the support is near the point of contact between the granular chain and the plate, the guided waves generated by the granular chain will return to their departing point during the contact time between the plate and the last particle in the chain. This means that the kinetic energy imparted to the plate upon the incidence of the solitary wave is partially retrieved, helping push the last sphere back and thus strengthening the reflected solitary waves. In contrast, if the plate support is remote the guided waves in the plate are not retrieved to the departure point during the contact period and thus the reflection of solitary waves becomes independent of the distance from the support.

The analytical prediction of the critical distance is challenging due to the dispersive nature of the propagating waves in the plate. Sondergaard *et al.* analytically predicted the critical distance for a single sphere impact on a plate based on the propagation of shear and Rayleigh waves on a semi-infinite block (Sondergaard et al., 1990). In reality, however, the guided waves in thin plates exhibit numerous Lamb wave modes with different group velocities. Figure 9 shows the first three Lamb wave modes in thin plates, with 'S' and 'A' denoting symmetric and asymmetric modes, respectively (Viktorov, 1967; Vallen Systeme GmbH). We find that the thin plate exhibits a wide range of group velocities, from below ~1,000 m/s for A_0 mode to ~5,000 m/s for S_0 mode in low frequencies. To account for different modes of Lamb wave propagation, we represent the propagation speed of dispersive waves by:

$$c = k\sqrt{E_p / \rho_p},\tag{17}$$

where k is a parameter that depends on the modes and frequencies of propagating Lamb waves. The contact time between the granular crystal and the plate is approximated to the contact time of a sphere against the half-spaced wall ($T_{c,0}$ in Eq. (7)) (Sondergaard et al., 1990). Thus, the critical distance L_c can be obtained by calculating the half transit distance of the guided waves during the contact time $T_{c,0}$:

$$L_c = \frac{cT_{c,0}}{2}$$
$$= 1.37 k\, D \left[\rho_s \left(\frac{1-v_s^2}{E_s} + \frac{1-v_p^2}{E_p} \right) \right]^{2/5} \sqrt{\frac{E_p}{\rho_p}} v_{imp}^{-1/5} .\tag{18}$$

As a result, Fig. 10 shows the relationship between the critical distances and the sphere diameters for different values of k based on Eq. (18). The black solid line represents the critical distance corresponding to the Rayleigh waves ($k = 0.57$ or $c \approx 2,900$ m/s), while the black dashed line denotes the critical distance based on the A_0-mode Lamb wave propagation ($k = 0.2$ or $c \approx 1,000$ m/s).

The experimental and numerical observations of the critical distances are also included in Fig. 10. We find that the analytical prediction based on the Rayleigh wave propagation overestimates the critical

distance in comparison to the experimental or numerical results. This suggests that the boundary effect is created by the guided waves slower than the Rayleigh waves. On the other hand, the critical distance based on the A_0-mode Lamb waves forms the upper boundary of the experimental and numerical results. We therefore expect that dispersive guided waves, with propagating speed between Rayleigh waves and ~1,000 m/s, are the primary guided waves that carry the majority of the kinetic energy and affect the rebounding motion of the granular chain at the interface. In Fig. 10, we find that the critical distance is not a sole function of sphere diameter, but also affected by the plate thickness. We observe that the thinner plate has longer critical distance, compared to the thicker plate, when identical sphere sizes are used in the granular crystals. This is probably due to the elongated contact time and thus, longer distance of wave propagation for a thin plate, as discussed in Sec. 4.1.

5. Conclusion

In this work, we investigate the interaction of highly nonlinear solitary waves with thin large plates. The solitary waves are formed and propagated in a one-dimensional chain of spherical particles, and interact with the plate structure via the mechanical contact in the orthogonal direction. In this process, the reflected solitary waves from the interface are significantly affected by the geometry and the boundary conditions of the plate. We find that the delay and attenuation of the reflected solitary waves result from the inelasticity inherent to large plates, caused by the dispersion of elastic waves in the plate. We analytically investigate this inelasticity effect in various geometrical configurations, using the classical plate theory and the contact mechanics. We also find that the coupling behavior between the granular chain and the plate is strongly affected by boundary conditions within some critical distance from the fixed support. By calculating the travelling distance of the dispersive guided waves in the plate during the estimated interaction time between the granular chain and the plate, we derive the critical distance in association with the granular chain and plate geometry. The experimental results are confirmed by the numerical approaches based on a combined discrete element and finite element model.

By leveraging the sensitivity of highly nonlinear solitary waves, one-dimensional granular crystals can be used as a nondestructive evaluation tool to assess the mechanical properties of plate structures. This sensor instrument can provide unique advantages, such as portability and energy efficiency, over conventional ultrasound-based schemes. In particular, the ability to predict solitary wave responses based on analytical schemes can lead to the development of an advanced diagnostic scheme without the need for baseline data, which is a major roadblock in many nondestructive evaluation applications.

References

Chatterjee, A., 1999. Asymptotic solution for solitary waves in a chain of elastic spheres. Physical Review E 59, 5912-5919.

Coste, C., Falcon, E., Fauve, S., 1997. Solitary waves in a chain of beads under Hertz contact. Physical Review E 56, 6104-6117.

Daraio, C., Nesterenko, V.F., Herbold, E.B., Jin, S., 2005. Strongly nonlinear waves in a chain of Teflon beads. Physical Review E 72, 016603.

Daraio, C., Nesterenko, V.F., Herbold, E.B., Jin, S., 2006a. Energy trapping and shock disintegration in a composite granular medium. Physical Review Letters 96, 058002.

Daraio, C., Nesterenko, V.F., Herbold, E.B., Jin, S., 2006b. Tunability of solitary wave properties in one-dimensional strongly nonlinear phononic crystals. Phys Rev E Stat Nonlin Soft Matter Phys 73, 026610.

Ha, S., 2009. Modeling Lamb Wave Propagation Induced by Adhesively Bonded PZTs on Thin Plates, Ph.D. Dissertation, Aeronautics and Astronautics. Stanford University, Stanford.

Hladky-Hennion, A.C., de Billy, M., 2007. Experimental validation of band gaps and localization in a one-dimensional diatomic phononic crystal. J Acoust Soc Am 122, 2594-2600.

Hong, J., 2005. Universal power-law decay of the impulse energy in granular protectors. Physical Review Letters 94, 108001.

Job, S., Melo, F., Sokolow, A., Sen, S., 2005. How Hertzian solitary waves interact with boundaries in a 1D granular medium. Physical Review Letters 94, 178002.

Job, S., Melo, F., Sokolow, A., Sen, S., 2007. Solitary wave trains in granular chains: experiments, theory and simulations. Granular Matter 10, 13-20.

Johnson, K.L., 1985. Contact Mechanics. Cambridge University Press.

Khatri, D., Rizzo, P., Daraio, C., 2008. Highly Nonlinear Waves' Sensor Technology for Highway Infrastructures, SPIE Smart Structures/NDE, 15th annual international symposium, San Diego, CA, pp. Manuscript number 6934-6925.

Kim, Y., Ha, S., Chang, F.-K., 2008. Time-Domain Spectral Element Method for Built-In Piezoelectric-Actuator-Induced Lamb Wave Propagation Analysis. AIAA Journal 46, 591-600.

Komatitsch, D., Barnes, C., Tromp, J., 2000. Simulation of anisotropic wave propagation based upon a spectral element method. Geophysics 65, 1251-1260.

Melo, F., Job, S., Santibanez, F., Tapia, F., 2006. Experimental evidence of shock mitigation in a Hertzian tapered chain. Physical Review E 73, 041305.

Nesterenko, V.F., 1983. Propagation of nonlinear compression pulses in granular media. Journal of Applied Mechanics and Technical Physics|Zhurnal Prikladnoi Mekhaniki i Tehknicheskoi Fiziki 24, 733-743|136-748.

Nesterenko, V.F., 2001. Dynamics of Heterogeneous Materials. Springer-Verlag New York, Inc, New York.

Ni, X., Rizzo, P., Daraio, C., 2011. Actuators for the generation of highly nonlinear solitary waves. Review of Scientific Instruments 82, 034902-034906.

Patera, A.T., 1984. A spectral element method for fluid dynamics: Laminar flow in a channel expansion. Journal of Computational Physics 54, 468-488.

Sen, S., Manciu, F.S., Manciu, M., 2001. Thermalizing an impulse. Physica A: Statistical Mechanics and its Applications 299, 551-558.

Sen, S., Manciu, M., Wright, J.D., 1998. Solitonlike pulses in perturbed and driven Hertzian chains and their possible applications in detecting buried impurities. Physical Review E 57, 2386-2397.

Sen, S., Mohan, T.R.K., Visco, D.P., Swaminathan, S., Sokolow, A., Avalos, A., Nakagawa, M., 2005. Using Mechanical Energy as a Probe for the Detection and Imaging of shallow Buried Inclusions in Dry Granular Beds. Int. J. Mod. Phys. B (Singapore) 19, 2951-2973.

Sinkovits, R.S., Sen, S., 1995. Nonlinear Dynamics in Granular Columns. Physical Review Letters 74, 2686-2689.

Sokolow, A., Bittle, E.G., Sen, S., 2007. Solitary wave train formation in Hertzian chains. EPL (Europhysics Letters) 77, 24002.

Sondergaard, R., Chaney, K., Brennen, C.E., 1990. Measurements of Solid Spheres Bouncing Off Flat Plates. J. Appl. Mech 57, 694-699.

Spadoni, A., Daraio, C., 2010. Generation and control of sound bullets with a nonlinear acoustic lens. Proc Natl Acad Sci U S A, 7230-7234.

Tillett, J.P.A., 1954. A study of the impact of spheres on plates. Proceedings of the Physical Society 67, 677-688.

Tournat, V., Gusev, V.E., 2010. Acoustics of Unconsolidated Model Granular Media: An Overview of Recent Results and Several Open Problems. Acta Acustica united with Acustica 96, 208-224.

Vallen Systeme GmbH, Schaeftlarner Weg 26, 82057 Icking, Germany (Software for wave dispersion silumations is downloadable from website: http://www.vallen.de/)

Viktorov, I., 1967. Rayleigh and Lamb Waves. Plenum Press, New York.

Yang, J., Silvestro, C., Khatri, D., De Nardo, L., Daraio, C., 2011. Interaction of highly nonlinear solitary waves with linear elastic media. Physical Review E 83, 046606.

Yang, J., Silvestro, C., Sangiorgio, S., Borkowski, S., Ebramzadeh, E., De Nardo, L., Daraio, C., 2012. Nondestructive evaluation of orthopedic implant stability in THA using highly nonlinear solitary waves. Smart Materials and Structures 21, 012001.

Zener, C., 1941. The Intrinsic Inelasticity of Large Plates. Physical Review 59, 669.

Zienkiewicz, O.C., Taylor, R.L., Zhu, J.Z., 2005. The Finite Element Method: Its Basis and Fundamentals, 6 ed. Butterworth-Heinemann.
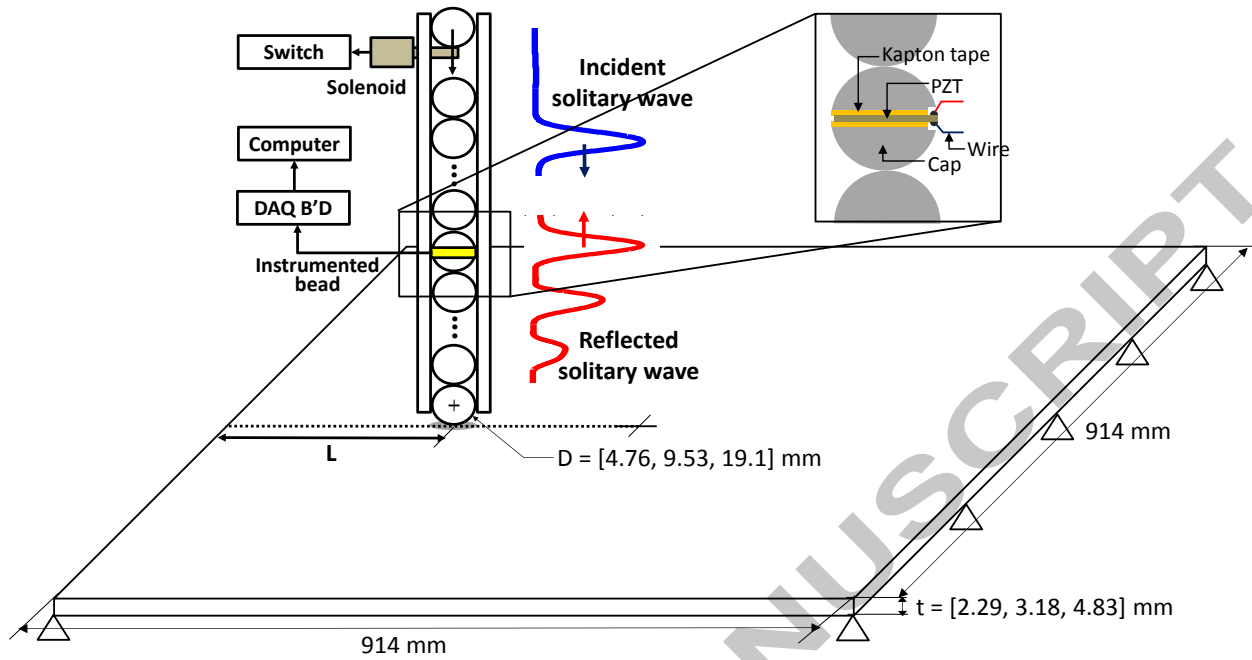
Fig. 1. Schematic of experimental setup. A one-dimensional granular chain composed of elastic spheres is positioned vertically along the dotted central line of an aluminum plate. A single solitary wave (blue line) is transmitted into the plate by releasing a striker from a 5-mm drop height using a solenoid. The reflected solitary waves (red line) are recorded by the instrumented bead (inset) positioned in the 7th particle from the top of the chain. The measured signals are transferred to a computer using a data acquisition board.

18
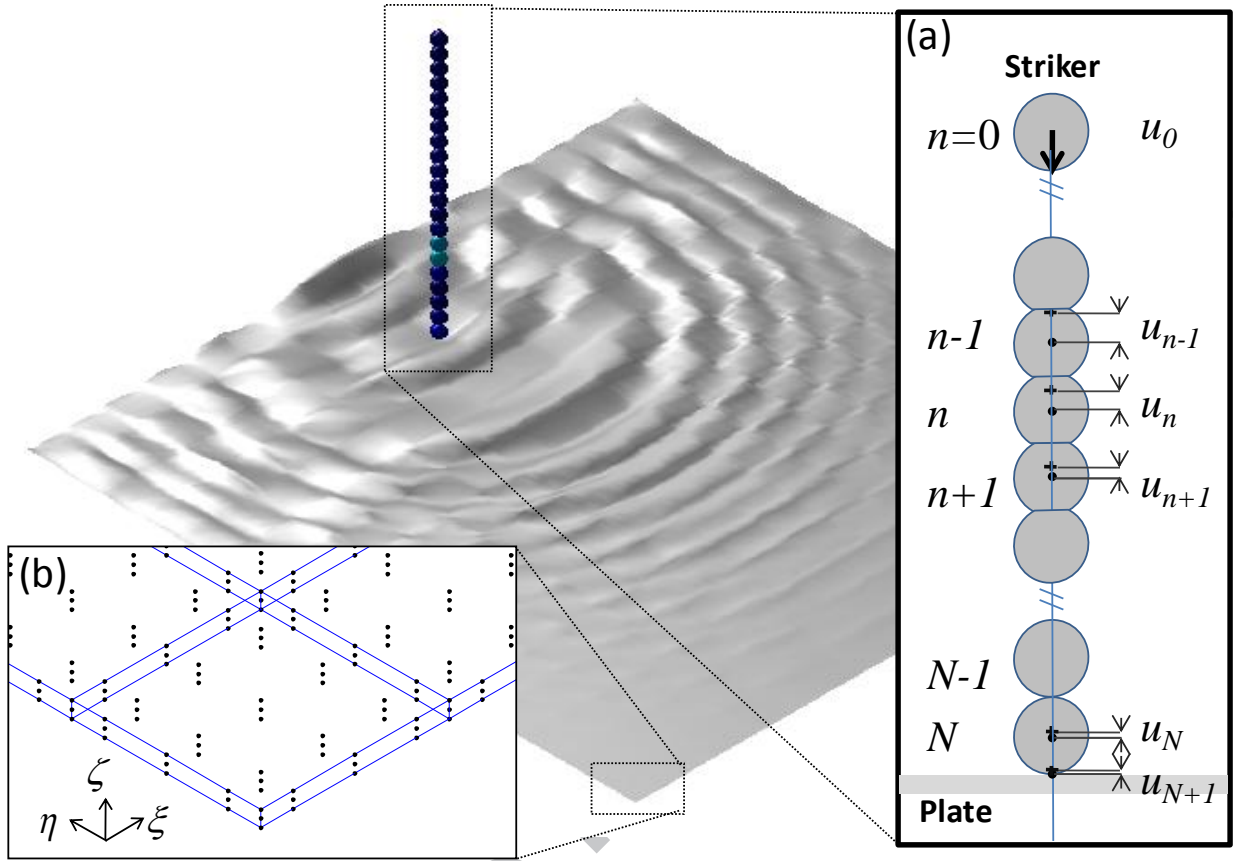
Fig. 2. Snapshot of guided wave propagation in the plate under the interaction with the granular chain, obtained from the combined DEM and SEM approach. (a) 1D chain of spheres in DEM for simulating nonlinear wave propagation. (b) Nodal distribution in SEM using the 4th-order GLL points in the horizontal direction and the 2nd-order GLL points in the vertical direction.
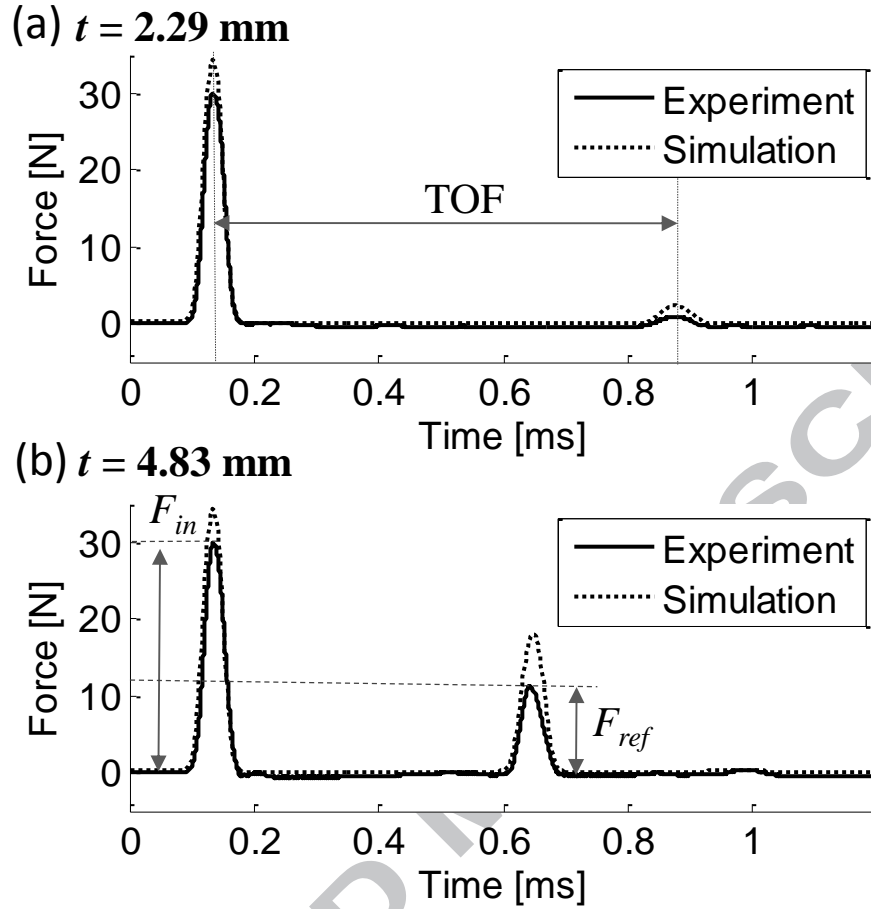
Fig. 3. Experimental and numerical profiles of solitary waves in the granular chain (D = 9.52 mm) under the interaction with two different plates. (a) Force profiles for a thin plate (t = 2.28 mm). (b) Force profiles for a thick plate (t = 9.52 mm). The reflected solitary waves against the thick plate exhibit a stronger (larger F_{ref}) and faster (smaller TOF) waveform compared to that of the thin plate.
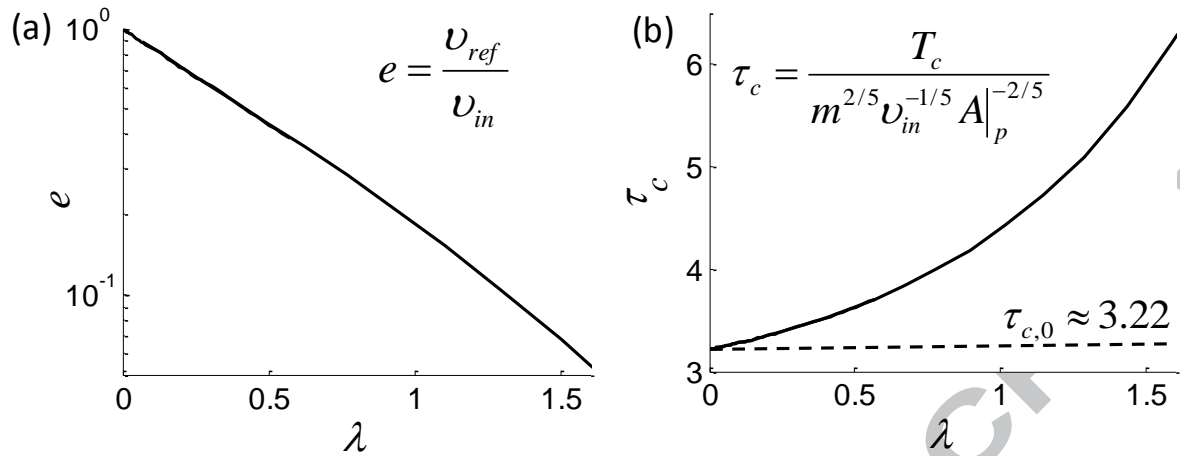
Fig. 4. Analytical description of a sphere reaction against a large plate. (a) Restitution coefficient (e) as a function of inelasticity parameter (λ). (b) Dimensionless contact time (τ_c) as a function of λ. If $\lambda = 0$ (corresponding to the elastic impact of a sphere against a half-spaced block), the dimensionless contact time approaches $\tau_c \approx 3.22$.
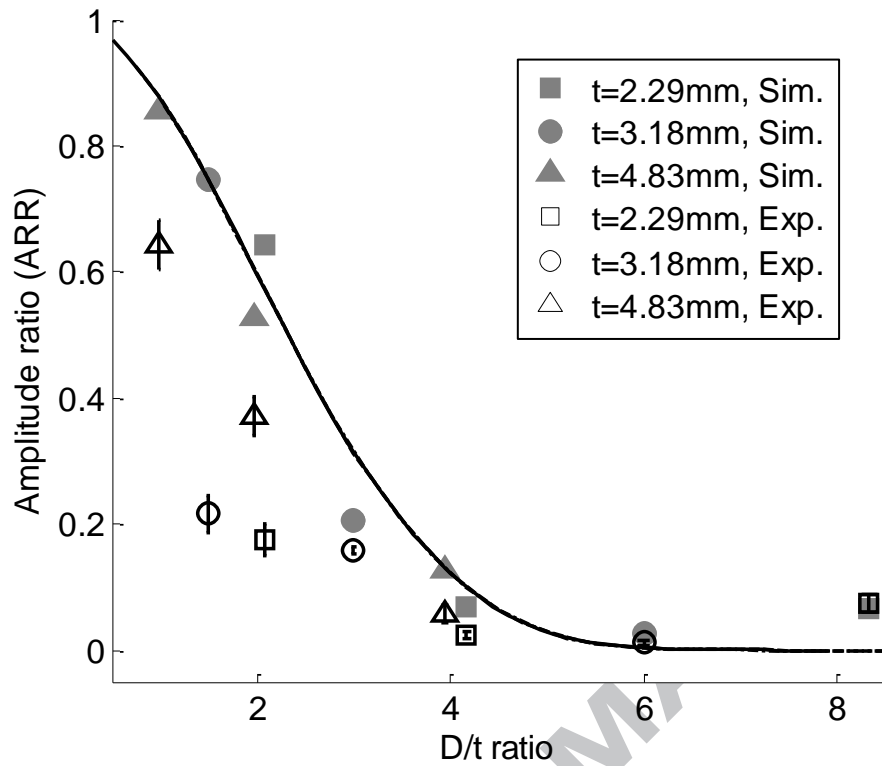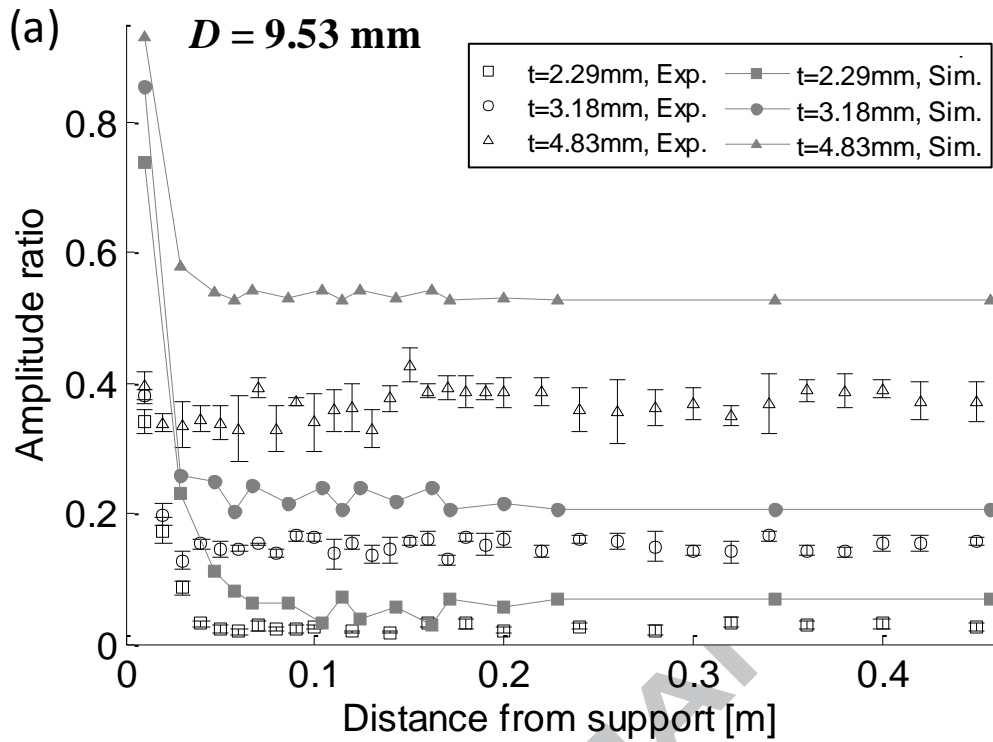
Fig. 5. Amplitude ratio of reflected solitary waves (ARR) as a function of the ratio of the sphere diameter to the plate thickness (*D/t*). The solid black line represents the analytical results, while the filled and hollow marks denote the numerical and experimental results, respectively. The ARR curve is a sole function of *D/t* rather than the individual dimensions of granular crystals and the plate.
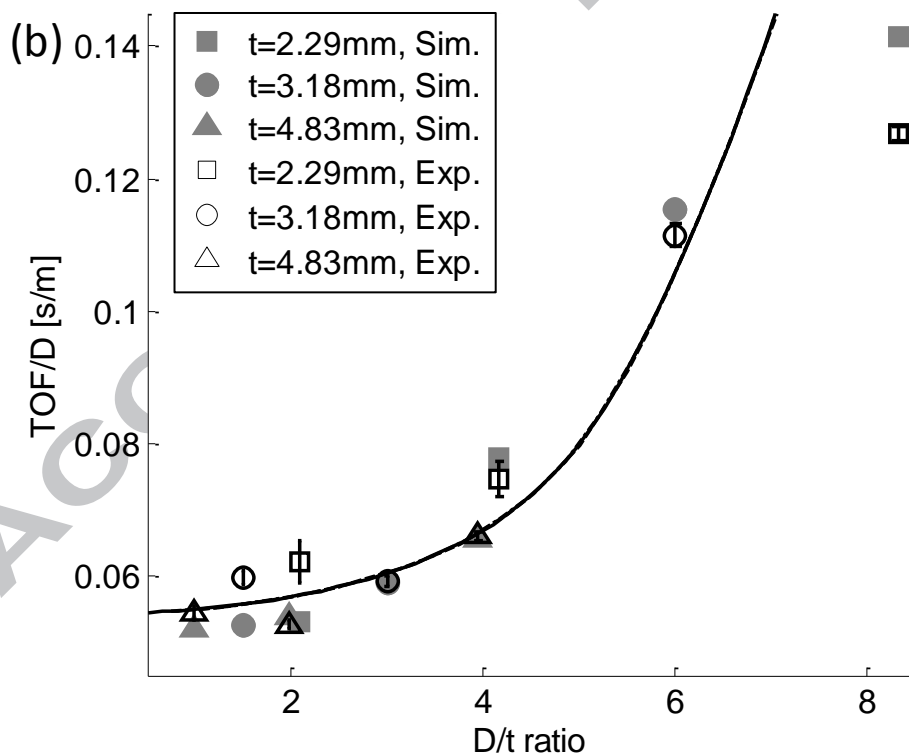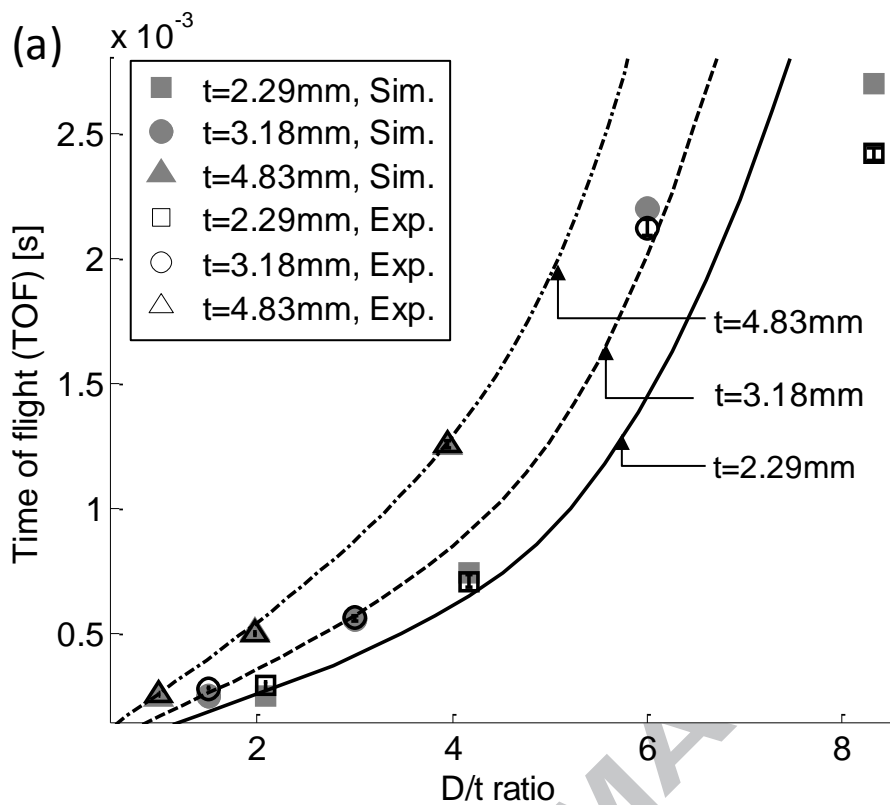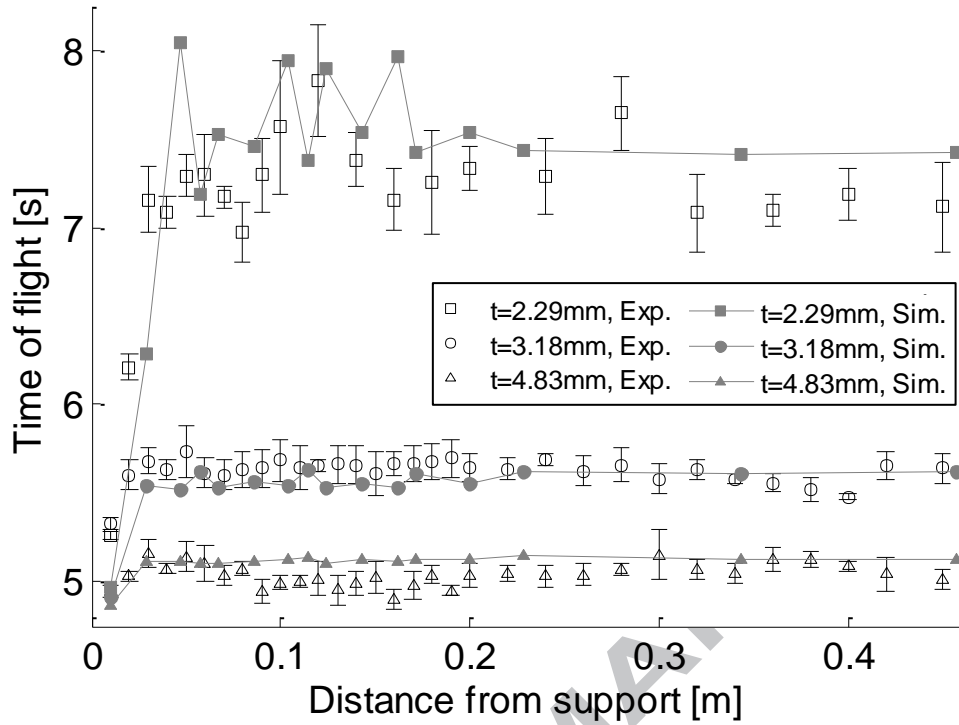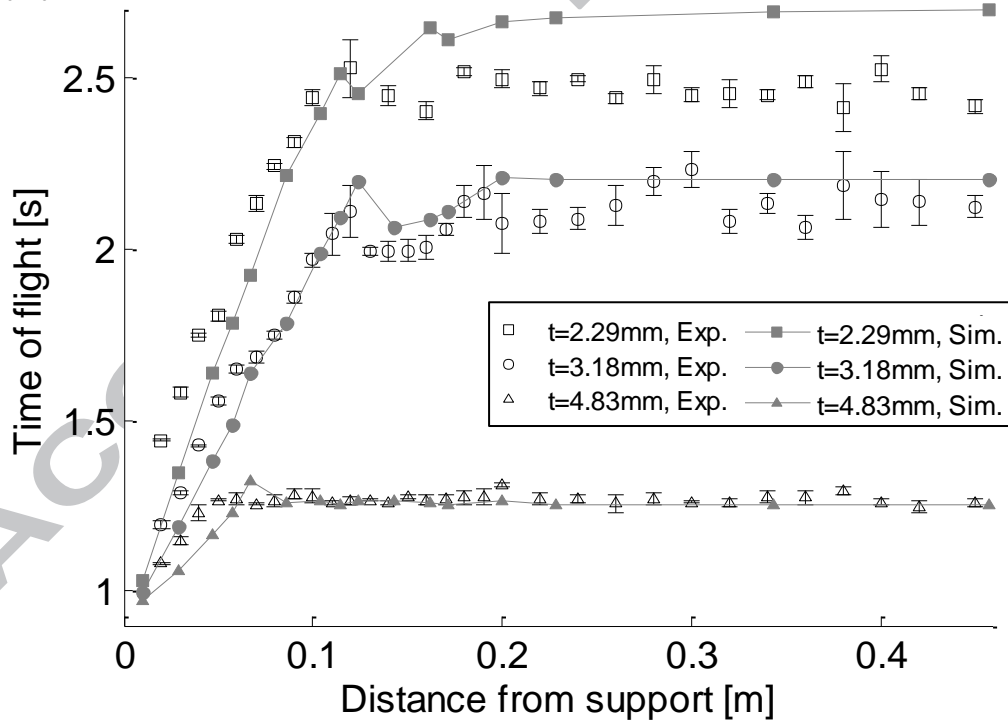
Fig. 6. (a) Time of flight (TOF) as a function of *D/t*. (b) Normalized TOF with respect to *D* as a function of *D/t*. After normalization, the three different curves in (a) overlap into a single curve in (b).
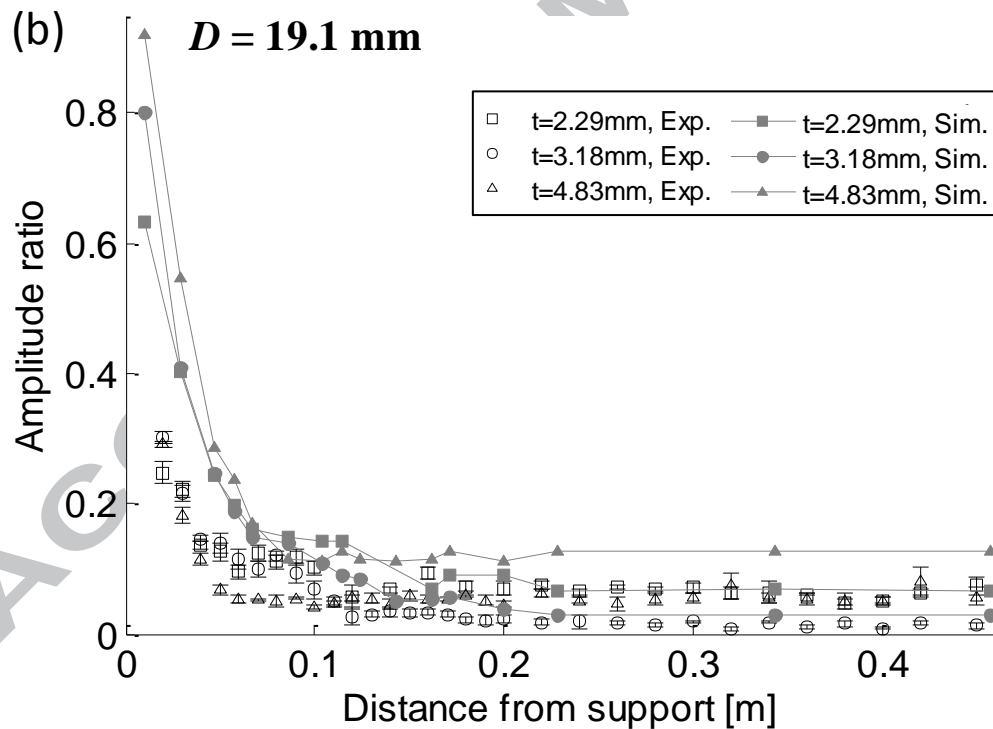
Fig. 7. Amplitude ratio of reflected solitary waves (ARR) as a function of distance from the support. (a) Granular chain with small spheres (D = 9.53 mm). (b) Granular chain with large spheres (D = 19.1 mm). Filled and hollow marks represent simulation and experimental results respectively. The error bars in experiments denote standard deviations based on five measurements of solitary wave signals.

Fig. 8. Time of flight (TOF) as a function of distance from the support. (a) Granular chain with small spheres (D = 9.53 mm). (b) Granular chain with large spheres (D = 19.1 mm).
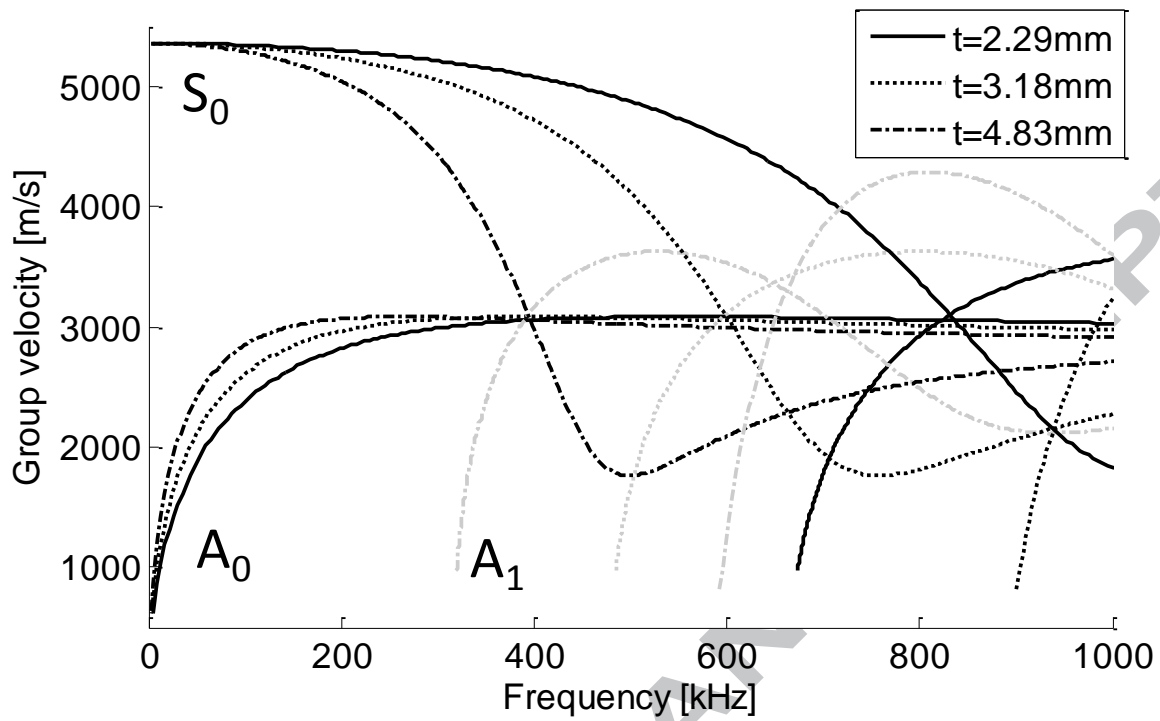
Fig. 9. Dispersion curves of guided waves in large aluminum plates with three different thickness (*t*). In low frequency region, the speed of the S_0-mode (first symmetric mode) wave is ~5,000 m/s, while that of the A_0-mode (first asymmetric mode) becomes less than 1,000 m/s.
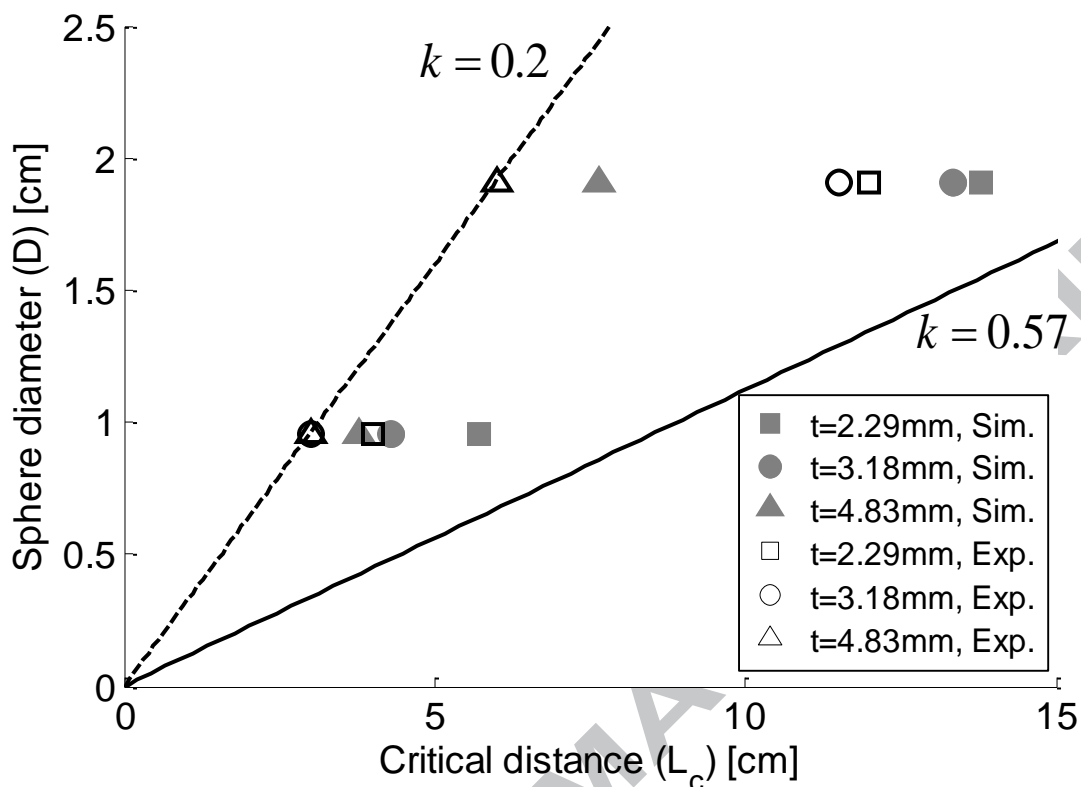
Fig. 10. Critical distances (L_c) in various thicknesses (t) of plates and the diameters (D) of granular crystals. Solid and dashed black lines denote the analytical predictions based on the propagation of guided waves with velocity parameter $k = 0.57$ and 0.2 (i.e., $c = 2,900$ and $1,000$ m/s), during the contact time $T_{c,0}$. The experimental and numerical results are represented by the hollow and filled marks.